Vietnam Journal of Catalysis and Adsorption
Tạp chí xúc tác và hấp phụ Việt Nam

http://chemeng.hust.edu.vn/jca/

A comparative study on the VOCs sensing behaviors of various ZnO nanostructures

Nguyen Minh Vuong*, Dinh Tien Dung, Hoang Nhat Hieu, Nguyen Van Nghia, Nguyen Ngoc Khoa Truong, Le Thi Ngoc Loan and Phan Thanh Hai

Faculty of Natural Sciences, Quy Nhon University, 170 An Duong Vuong, Quy Nhon, Binh Dinh, Vietnam
**Email: nmvuongk23@gmail.com or nguyenminhvuong@qnu.edu.vn*

ARTICLE INFO

Received: 15/10/2020
Accepted: 30/12/2020

Keywords: VOCs sensing, ZnO, nanostructure, open space, electrospinning

ABSTRACT

The volatile organic compounds (VOCs) sensing layers were studied using ZnO nanomaterials with different morphologies including hierarchical nanostructure (ZnO-H), nanorods (ZnO-NRs), commercial nanoparticles (ZnO-CNPs) and wet chemical synthesized nanoparticles (ZnO-HNPs). ZnO hierarchical structure was fabricated by an electrospinning technique followed by hydrothermal process. ZnO vertical nanorods structure was fabricated by hydrothermal method, while ZnO nanoparticles based sensors were prepared from commercial powder and wet chemical method. The morphology and properties of the fabricated samples were examined by scanning electron microscopy (SEM), X-ray diffraction (XRD) and transmission electron microscopy (TEM). VOCs sensing responses toward acetone, ethanol and methanol with respect to altered ZnO nanostructures was systematically compared at different working temperatures. The enhanced response at low working temperatures induced by the open space hierarchical structure was observed. The VOCs sensing mechanisms of the ZnO nanostructures based sensing layer were also explained and discussed in detail.

Introduction

Nanostructured semiconducting metal oxides gas/vapor sensors have been studied intensively over the years due to their practical applications in everyday life, as well as in environmental protection, bio detection, just to name a few. In comparison to other metal oxide nanomaterials such as WO_3, TiO_2, SnO_2, gas/vapor sensors based on ZnO nanostructures have attracted much attention because of their advantageous properties such as low cost, high response, high electron mobility, good chemical/ thermal stability and diverse morphologies, i.e. nanowires, nanofibers, nanorods, nanoparticles, nanosheets and nanobelts [1-4]. Gas adsorption/ desorption processes occur mainly on the surface of sensing layers. The performance of gas/vapor sensors can be tuned by modification of the sensing layers. These strategies consist of surface modification, hybridization and light illumination during sensing measurement [5-12]. Moreover, the response of gas sensor is strongly dependent on the morphology, porosity, and crystalline size of the sensing layers. Specially, significant improvement of the sensor's performance was obtained by the nanostructures with high porosity owning a larger number of active sites and crystalline size closing by the complete depletion condition [13].

In our previous study [14], a facile strategy for the fabrication of ZnO-H nanostructure with high porosity

http://doi.org/10.51316/jca.2020.080

intended for sensing performance improvement was reported. Herein, ZnO nanorods were successfully grown around the ZnO nanofibers upon employing electrospinning technique. In the present work, a comparable study on ZnO nanostructures based sensors with various morphologies consisting of hierarchical nanostructure (ZnO-H), nanorods (ZnO-NRs), commercial nanoparticles (ZnO-CNPs) and wet chemical synthesized nanoparticles (ZnO-HNPs), towards VOCs (such as acetone, ethanol and methanol) is carried out. Consequently, the ZnO-H based nanostructure was assigned as the optimal one applied for sensing layer due to the noticeable improvement in the sensor response with respect to almost tested VOCs at low working temperature. This finding opens a new avenue to employ the open space hierarchical structure of semiconducting metal oxides as the gas sensing layers with the aim at improving the sensing performance of VOCs.

Experimental

All chemicals including Polyvinylpyrrolidone (PVP) (wt 360000), Zinc acetatedihydrate (ZnAc) ($Zn(CH_3COO)_2{\cdot}2H_2O$, 99.99%), Zinc nitrate hexahydrate ($Zn(NO_3)_2.6H_2O$, 98%), DI water (18.4 MΩ/cm), N,N-dimethylformamide (DMF), Ethyl alcohol (C_2H_5OH), Hexamethylenetetramine (HMTA) ($C_2H_{12}N_4$, 99%), commercial ZnO nanoparticles and Dimethyl Sulfoxide (DMSO) were purchased from Sigma-Aldrich Co., Ltd and utilized without further purification. Preparation of ZnO-H nanostructure on sensing substrate is described as our previous work [14]. In the case of ZnO-NRs sensors, a ZnO seed layer was prepared on Au patterned Al_2O_3 substrates before ZnO vertical nanorods growth. Zinc contained solution, which consists dimethylformamide (3 ml), ethanol (2 ml), polyvinylpyrrolidone (PVP) (0.7 g) and zinc acetate (0.6 g), was spin-coated on sensing substrate for 1 min at the rotary rate of 3000 rpm. The sample was then annealed in air at 450°C for 2 hours to remove PVP and form ZnO seed layer. Hydrothermal conditions for ZnO nanorods fabrication are similar to those applied for ZnO-H. For preparation of sensors based on ZnO commercial nanoparticles (ZnO-CNPs), ZnO powder (particle size < 200 nm) was dispersed in acetic acid solution (0.1 M) at room temperature followed by spin-coat on Au patterned Al_2O_3 substrate at the rotary rate of 2000 rpm. In the case of ZnO-HNPs based sensor, zinc acetate (1M) was initially dissolved in dymethyl sulfoxide (DMSO) solvent to form a homogeneous solution. 30ml of DMSO is then heated to a specified temperature of 180°C. In the next step, 1 mL of zinc acetate solution was sprayed directly into the DMSO solution which was stirred and heated for ten minutes. The reaction solution was then fed into a centrifuge system at 6000 rpm to separate the ZnO nanoparticles from the solution. The observed ZnO nanoparticles were washed with ethanol and centrifuged 3 times to remove solvents and dissolved impurities. Finally, ZnO nanoparticles were dispersed in ethanol and coated on the sensor substrate. These fabricated sensors were also annealed in air at 500°C for 2 h for stabilizing the ZnO-H, ZnO-NRs, ZnO-CNPs and ZnO-HNPs structures on the sensing substrates.

The surface morphology of the fabricated materials was investigated by scanning electron microscopy (SEM, LYRA3-XMU). The structural property was investigated by X-ray diffraction (XRD RigakuRTP300) using Cu Kα radiation with a Ni filter and transmission electron microscopy (TEM). The VOCs sensing properties of the fabricated sensors were characterized in a home-built measurement system using an ammeter/voltage source unit (Keithley 2601B). Dry air was used as the carrier and dilution gas. Since acetone, ethanol and methanol are liquid at room temperature, a bubbler evaporation system was employed to deliver the controlled acetone concentration to the detection chamber.

Results and discussion

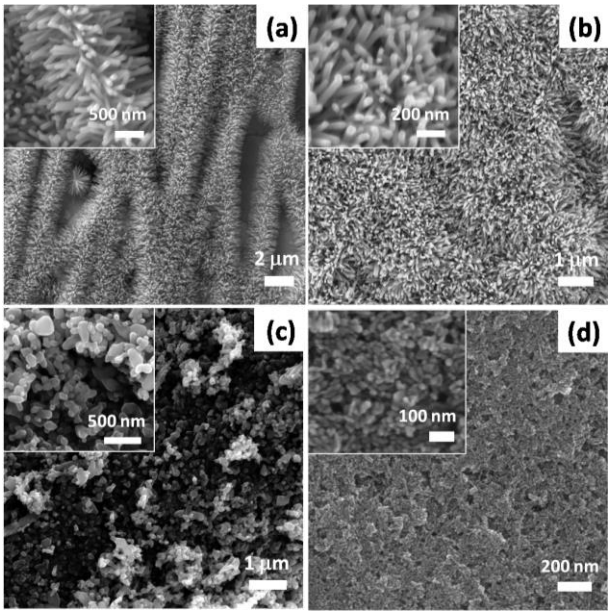

Figure 1: SEM images of the ZnO-H (a), ZnO-NRs (b), ZnO-CNPs structures (c) and ZnO-HNPs. Insets show high magnification SEM images

Fig. 1a shows an SEM image of the ZnO-H structure obtained by hydrothermal growth of ZnO nanorods on

the templated ZnO nanofibers. The secondary ZnO nanorods forming from hydrothermal growth are organized into very regular arrays symmetrically around the ZnO nanofibers to form as bunches with the so-called squirrel's tail like shape. The ZnO nanorods grown from different bunches and rod-rod contacts in the same bunches can link each other to form the electric pathways between two Au electrodes, acting as a gas/vapor sensing layer for the resistance measurement. The high porosity in this ZnO-H structure was expected to improve the performance of gas/vapor sensor because they enable gases to freely flow and react with the entire surface of ZnO material in term of minimal diffusion effect [13]. A high-magnification SEM image (inset in Fig. 2a) reveals that the diameter and the length of the ZnO nanorods are in the range of 40 – 60 nm and ~ 1 µm, respectively. Fig. 1b shows an SEM image of the ZnO-NRs structures in which the ZnO nanorods are randomly oriented and non-perpendicular to the substrate. The rod-rod contacts, which play a role as the conducting channels in the sensing layer, are also recorded. The ZnO-CNPs nanostructures created sensing layer is illustrated in Fig. 1c. ZnO-CNPs exhibit a wide distribution of sizes from 30 nm up to 150 nm. Whereas, ZnO-HNPs reveals a narrower distribution of particle size from 20 to 35 nm (Fig. 1d).

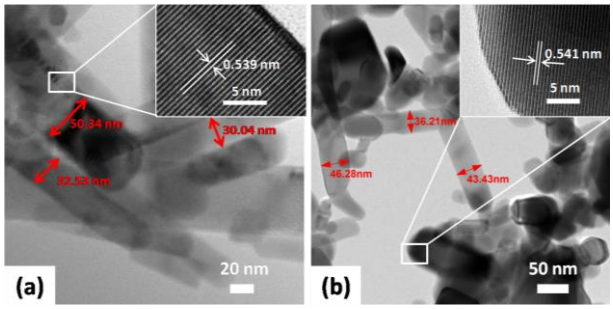

Figure 2: TEM and HRTEM (inset) images of ZnO-H (a) and ZnO- CNPs (b) structures

TEM images of ZnO nanorods in ZnO-H structure and ZnO nanoparticles in ZnO-CNPs structure are shown in Figs. 2a and 2b, respectively. The diameter of nanorods (Fig. 2a) and nanoparticles (Fig. 2b) is in line with the analyzed SEM results mentioned above. The growth direction of the nanorods in ZnO-H structure is confirmed by high-resolution TEM image, shown in Fig. 2 (insets), which reveals well-resolved fringes in the dimensions perpendicular to the nanorods axis. It is also further confirmed that the nanorod is single crystalline. The lattice fringe spaces are measured to be 0.539 nm and 0.541 nm for ZnO-H and ZnO-CNPs, respectively, matching well with the interplanar spacing of the (001) plane of hexagonal wurtzite ZnO crystal.

The XRD patterns of the ZnO-H, ZnO-NRs, ZnO-CNPs and ZnO-HNPs structures prepared on glass substrates are compared in Fig. 3. The morphologies of these structures on both Al_2O_3 and glass substrates are similar exhibiting a highly crystalline hexagonal wurtzite tructure with the lattice parameters of a = 3.25 Å and c = 5.21 Å [JCPDS 36-1451]. The diffraction peaks in ZnO-H and ZnO-NRs structures with stronger intensity are centered at a scattering angle of 34.5°, which correspond to the (002) diffraction plane of the wurtzite type of ZnO. This result provides a firm evidence that the growth process of ZnO nanorods is highly oriented in the <001> direction.

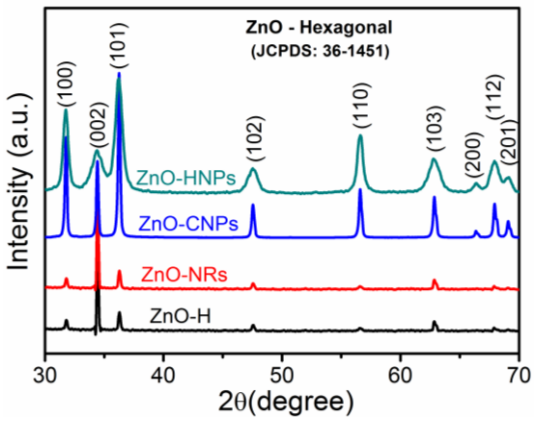

Figure 3: XRD patterns of ZnO-H, ZnO-NRs, ZnO-CNPs and ZnO-HNPs structures

To study the sensing properties of the fabricated sensors toward acetone vapor, the response of the ZnO-H, ZnO-NRs, ZnO-CNPs, and ZnO-HNPs upon exposed to acetone vapor 1.86 % in dry air at different working temperatures (220-300°C) were investigated (Fig. 4). The response is defined by the R_i/R_g ratio, where R_i is the sensor's resistance in air ambient and R_g is the resistance upon exposure to target gas at a given working temperature. Accordingly, the responses of all sensors increase with increasing working temperature. The optimal working temperature of the sensors ZnO-H, ZnO-NRs and ZnO-CNPs was determined at 280°C and of ZnO-HNPs sensor is 240°C. At the optimum working temperature, the highest response of the ZnO-H, ZnO-NRs, ZnO-CNPs and ZnO-HNPs sensors was 11000%, 920%, 960% and 1220%, respectively. The ZnO-H sensor shows a significantly improved response compared to that of the sensors based on ZnO-NRs, ZnO-CNPs, and ZnO-CNPs at all measured working temperatures.

http://doi.org/10.51316/jca.2020.080

Likewise, in order to investigate the sensing properties toward ethanol vapor, the response properties of the sensors based on ZnO-H, ZnO-NRs, ZnO-CNPs and ZnO-HNPs when exposed to ethanol vapor 0.477 % in dry air at different working temperatures (220-300°C) are measured and shown in Fig. 5. As a result, the response of all sensors increases with increasing working temperature. The optimum working temperature of the ZnO-H and ZnO-HNPs sensors is determined to be 260°C. Meanwhile, the optimum working temperatures of 280°C and 300°C are accounted for the ZnO-NRs and ZnO-CNPs sensors respectively.

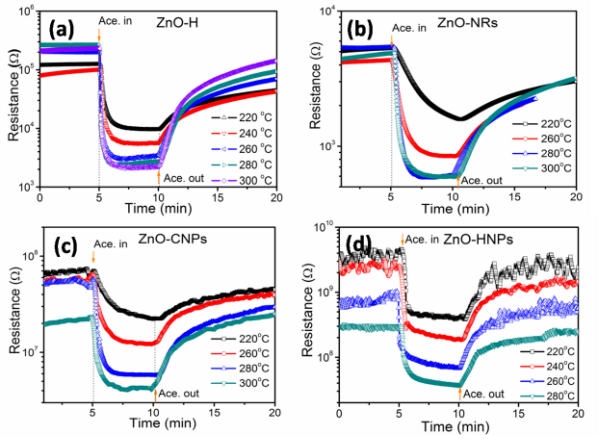

Figure 4: The response properties upon exposure to 1.86% acetone vapor in dry air at different working temperatures of ZnO-H (a), ZnO-NRs (b), ZnO-CNPs (c) and ZnO-HNPs (c)

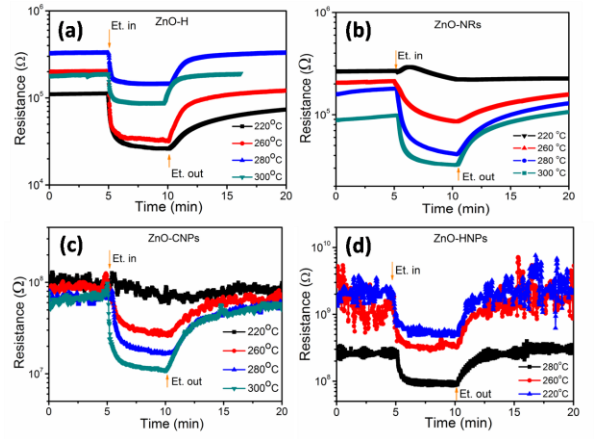

Figure 5: The resistance behavior of ZnO-H (a), ZnO-NRs (b), ZnO-CNPs (c) and ZnO-HNPs (d) sensors upon exposure to 0.477% ethanol vapor in dry air at different working temperatures

Note, due to the limitation of the measuring system the working temperature is restricted below 300°C. With respect to the ZnO-HNPs based sensor, although the highest response is at 260°C, the resistive type response curve is somehow noisy (due to high resistance). At the optimum working temperature, the highest response of ZnO-H, ZnO-NRs, ZnO-CNPs and ZnO-HNPs sensors is of 640%, 416%, 620% and 270%, respectively. The response of sensor based on the ZnO-H structure shows a significant improvement compared to that of sensors based on ZnO-NRs, ZnO-CNPs and ZnO-CNPs at all working temperatures less than 260°C.

The methanol sensing properties of the fabricated sensors also measured under exposure to concentration of 1.03 % in dry air at different working temperatures (220-300°C) (Fig. 6). The results showed that the response of all sensors increase with increasing working temperature. While the optimum working temperatures of the sensors ZnO-H, ZnO-NRs and ZnO-HNPs were determined at 260°C, 300°C and 280°C, respectively. The ZnO-CNPs sensor is almost insensitive to methanol vapor at the measured temperatures. This tentative conclusion is figured out upon testing a dozen of sample under the same conditions. Further investigations are obligated to disclose this phenomenon. At the optimum working temperature, the highest response of ZnO-H, ZnO-NRs and ZnO-HNPs based sensors is 5150%, 610% and 460% respectively. The response of sensors based on the ZnO-H structure also shows a significant improvement in comparison with that of other sensors at most of the measured working temperatures.

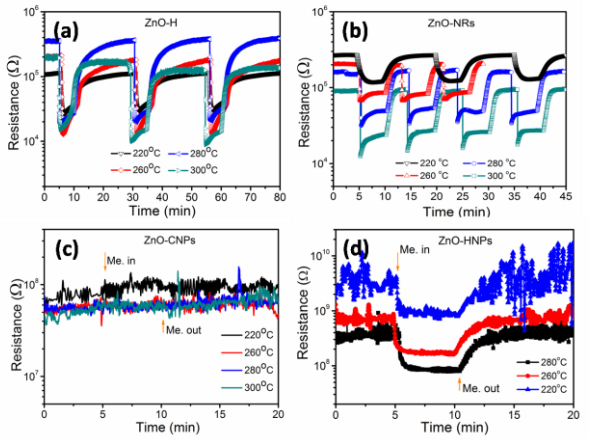

Figure 6: The resistance behavior of ZnO-H (a), ZnO-NRs (b), ZnO-CNPs (c) and ZnO-HNPs (d) based sensors upon exposure to 1.03% methanol vapor in dry air at different working temperatures.

Both sensors behaved as typical n-type semiconductor because the resistance decreased with exposure to the VOCs vapors. The gas sensing properties of these sensors can be explained by the ionosorption model

http://doi.org/10.51316/jca.2020.080

and the semiconductor junction theory [15]. When ZnO materials are exposed to dry air, the oxygen molecules adsorbing on ZnO surface enable capturing electrons in the conduction band of ZnO to form such ionic manners, i.e. O^{2-}, O^{-}, and O^{-2}. This ionosorption of oxygen narrows the conduction channel and hence increases the resistance of the sensor. When the sensor is exposed to VOCs vapor, VOCs molecules react with the absorbed oxygen ions on ZnO surface as the following equations [16]:

$$CH_3COCH_3 + 8O^-_{(ads)} \rightarrow 3CO_2 + 3H_2O + 8e^-,$$

$$C_2H_5OH + 6O^-_{(ads)} \rightarrow 2CO_2 + 3H_2O + 6e^-,$$

$$2CH_3OH + 6O^-_{(ads)} \rightarrow 2CO_2 + 4H_2O + 6e^-$$

thereby, decreasing the resistance of the sensor.

The highest response was obtained for sensors constructed by the ZnO-H structures in all three measured gases. More importantly,, the working temperature of ZnO-H structure for acetone vapor (280°C) is relatively lower than that reported in theprevious studies [17-20]. The enhanced response of ZnO-H structures compared with other structures can be attributed to the unique open-space porous ZnO-H structure. Hence, the gas and/or vapor could freely flow and contact the sensing layer surface with minimal diffusion effect [13]. Furthermore, the hierarchical structure was constructed on the basis of one-dimensional nanorods bearing a highly geometrical ratio. On the other hand, the former experimental research results and the molecular kinetics simulation theory confirmed that the ZnO crystal face $(10\bar{1}0)$ has a higher ability to adsorb VOCs gas molecules than other ZnO crystals, such as (0001), $(11\bar{2}0)$, ...[21]. This implies that the sensor with an open space structure (a case study of ZnO nanorods synthesized around the ZnO fiber) is likely to give a higher response than the rest of the structures. The open space structure is therefore found to be a potential structure used for gas sensor sensitive layers with the aim at improving the sensitivity performance of VOCs.

Conclusion

VOCs vapor sensors based on ZnO nanostructures with various morphologies were studied. VOCs vapor sensing properties of ZnO-H structure were performed and compared to those of ZnO-NRs, ZnO-CNPs and ZnO-HNPs structures. The optimal sensor structure is determined to be ZnO hierarchical structure. The responses of ZnO-H nanostructure based sensor towards VOCs vapors are obviously higher than other structures at the optimal working temperature. The VOCs vapor sensing mechanism of sensors is also explained in detail in terms of the surface reactions of ZnO upon exposure to VOCs vapor diluted by dry air. This finding opens a new avenue to employ the open space hierarchical structure of ZnO as the gas sensing layers with the aim at improving the sensing performance of VOCs.

Acknowledgments

This research is funded by Vietnam National Foundation for Science and Technology Development (NAFOSTED) under grant number 103.02-2017.77.

References

1. F.M. Li, G. Hsieh, S. Dalal, M.C. Newton, J.E. Stott, P. Hiralal, A. Nathan, P.A. Warburton, H.E. Unalan, P. Beecher, A.J. Flewitt, I. Robinson, G. Amaratunga, W.I. Milne, IEEE Transactions on Electron Devices 55 (2008) 3001. https://doi.org/10.1109/ted.2008.2005180
2. E. Çetinörgü, S. Goldsmith, Journal of Physics D: Applied Physics 40 (2007) 5220.
3. R. Dom, H.G. Kim, P.H. Borse, CrystEngComm 16 (2014) 2432. https://doi.org/10.1039/c3ce42058b
4. M.R. Alenezi, S.J. Henley, N.G. Emerson, S.R.P. Silva, Nanoscale 6 (2014) 235. 10.1039/c3nr04519f
5. W.J. Moon, J.H. Yu, G.M. Choi, Sensors and Actuators B: Chemical 87 (2002) 464. https://doi.org/10.1016/S0925-4005(02)00299-X
6. J. Huang, Y. Dai, C. Gu, Y. Sun, J. Liu, Journal of Alloys and Compounds 575 (2013) 115. https://doi.org/10.1016/j.jallcom.2013.04.094
7. N.M. Vuong, N.M. Hieu, H.N. Hieu, H. Yi, D. Kim, Y.-S. Han, M. Kim, Sensors and Actuators B: Chemical 192 (2014) 327. https://doi.org/10.1016/j.snb.2013.10.117
8. X. Liu, J. Sun, X. Zhang, Sensors and Actuators B: Chemical 211 (2015) 220. https://doi.org/10.1016/j.snb.2015.01.083
9. N. Hongsith, C. Viriyaworasakul, P. Mangkorntong, N. Mangkorntong, S. Choopun, Ceramics International 34 (2008) 823. https://doi.org/10.1016/j.ceramint.2007.09.099
10. Y. Li, J. Gong, G. He, Y. Deng, Materials Chemistry and Physics 134 (2012) 1172. http://dx.doi.org/10.1016/j.matchemphys.2012.04.014
11. Y. Mun, S. Park, S. An, C. Lee, H.W. Kim, Ceramics International 39 (2013) 8615. http://dx.doi.org/10.1016/j.ceramint.2013.04.035
12. I. Karaduman, D.E. Yıldız, M.M. Sincar, S. Acar, Materials Science in Semiconductor Processing 28

(2014) 43. http://dx.doi.org/10.1016/j.mssp.2014.04.011
13. N.M. Vuong, H. Jung, D. Kim, H. Kim, S.-K. Hong, Journal of Materials Chemistry 22 (2012) 6716. https://doi.org/10.1039/C2JM15971F
14. N.M. Vuong, N.D. Chinh, B.T. Huy, Y.-I. Lee, Scientific Reports 6 (2016) 26736. 10.1038/srep26736
15. https://www.nature.com/articles/srep26736#supplementary-information
16. N. Barsan, U. Weimar, Journal of Electroceramics 7 (2001) 143. https://doi.org/10.1023/a:1014405811371
17. X. Ma, X. Zhou, Y. Gong, N. Han, H. Liu, Y. Chen, RSC Advances 7 (2017) 34609. https://doi.org/10.1039/c7ra04437b
18. L. Shi, A.J.T. Naik, J.B.M. Goodall, C. Tighe, R. Gruar, R. Binions, I. Parkin, J. Darr, Langmuir 29 (2013) https://doi.org/10603. 10.1021/la402339m
19. P. Rai, Y.-S. Kim, H.-M. Song, M.-K. Song, Y.-T. Yu, Sensors and Actuators B: Chemical 165 (2012) 133. https://doi.org/10.1016/j.snb.2012.02.030
20. A.Z. Sadek, W. Wlodarski, K. Kalantar-zadeh, S. Choopun, ZnO Nanobelt Based Conductometric H2 and NO_2 Gas Sensors, SENSORS, 2005 IEEE, (2005) 1326.
21. S. Bai, L. Chen, S. Chen, R. Luo, D. Li, A. Chen, C.C. Liu, Sensors and Actuators B: Chemical 190 (2014) 760. https://doi.org/10.1016/j.snb.2013.09.032
22. Y.V. Kaneti, J. Yue, X. Jiang, A. Yu, The Journal of Physical Chemistry C 117 (2013) 13153. https://doi.org/10.1021/jp404329q